

Copyright © 2007. Reprinted from APPLIED PHYSICS LETTERS 91, 091901 .2007. Such permission of the American Institute of Physics does not in any way imply the American Institute of Physics endorsement of any of Institute of Microelectronics' products or services. Internal or personal use of this material is permitted. However, permission to reprint/republish this material for advertising or promotional purposes or for creating new collective works for resale or redistribution must be obtained from the American Institute of Physics by writing to Rights@aip.org.

Effects of alloying and localized electronic states on the resonant Raman spectra of $\text{Zn}_{1-x}\text{Mg}_x\text{O}$ nanocrystals

J. D. Ye,^{a)} K. W. Teoh, X. W. Sun,^{b)} G. Q. Lo, and D. L. Kwong
Institute of Microelectronics (IME), 11 Science Park Road, 117685 Singapore, Singapore

H. Zhao, S. L. Gu, R. Zhang, and Y. D. Zheng
Department of Physics, Nanjing University, Nanjing, 210093, People Republic of China

S. A. Oh, X. H. Zhang, and S. Tripathy^{c)}
Institute of Materials Research and Engineering (IMRE), 3 Research Link, 117602 Singapore, Singapore

(Received 9 July 2007; accepted 3 August 2007; published online 27 August 2007)

Using resonant Raman spectroscopy, the authors report on the alloying effect and localization of electronic states in $\text{Zn}_{1-x}\text{Mg}_x\text{O}$ ($x < 0.15$) nanostructures with average sizes in the range of 20–150 nm. Anomalous intensity enhancement of the second-order longitudinal optical phonon has been observed, which is due to Fröhlich interaction via the localized exciton as the resonant intermediate electronic states. The alloying-induced disorder due to Mg incorporation led to the enhancement of exciton localization as well as the asymmetric broadening of longitudinal optical phonon line shape. The composition in ZnMgO could be determined by the first-order longitudinal optical phonon frequency via a bowinglike quadratic fit. This simple relationship is in perfect match to the modified random-element-isodisplacement model and provides a nondestructive approach to probe the quantitative composition distributions in wurtzite ZnMgO alloy system. © 2007 American Institute of Physics. [DOI: 10.1063/1.2775813]

Recently, ZnMgO alloy system has been extensively studied for the understanding of fundamental physics in ZnMgO/ZnO-based heterostructures and quantum wells.^{1,2} Generally, in the ternary alloy system, atoms of the constituent binary semiconductors are randomly distributed, leading to fluctuations in masses and force constants in the neighborhood, which is known as alloying effect. Resonant Raman scattering (RRS) is a powerful technique to investigate the interband electronic transitions, excitons, and electron-phonon interactions in semiconductors, and has been widely studied for semiconductors alloy systems.^{3–5} Although Raman scattering under off-resonance or resonance conditions has been used to probe ZnO-based micro- and nanostructures, few efforts were made to investigate the alloying effects in the ZnMgO system.^{6–12} In this letter, we shall study the alloying effect and electronic states localization in $\text{Zn}_{1-x}\text{Mg}_x$ ($x < 0.15$) alloy via optical phonons in RRS probe. An anomalous intensity enhancement of the second-order longitudinal optical (LO) phonon has been observed due to the localized exciton-mediated Fröhlich interaction. The composition dependent asymmetric broadening and frequency shift of first-order longitudinal optical (1LO) phonons in these $\text{Zn}_{1-x}\text{Mg}_x\text{O}$ structures are studied in detail.

ZnO and MgO multilayers were prepared on Si (100) substrate at room temperature by electron-beam evaporation system using MgO (5N) and ZnO (5N) pieces as the sources. The as-deposited multilayer film (sample A) consisted of alternating MgO and ZnO layers with thicknesses of about 15 nm for each layer and about 450 nm for the total stack. The embedded as-grown ZnO nanocrystals are found to be of

spherical shape with an average size of ~ 7 nm. The ZnMgO nanocrystals were formed via thermal solid state diffusion at the ZnO/MgO interface by annealing of the multilayer film at 450, 600, 750, 900, and 1050 °C for 60 min in oxygen ambient, which are referred as samples B–F, respectively. These alloyed nanocrystals were distributed uniformly, as evidenced by electron microscopy, and their average sizes increased from 20 to 150 nm as the annealing temperature increased from 450 to 1050 °C. The x-ray diffraction results (not shown here) exhibited that the $\text{Zn}_{1-x}\text{Mg}_x\text{O}$ alloys were of wurtzite structures with low Mg composition ranging from $x=0.02$ to $x=0.14$, and the lattice constant c well agreed with the Vegards law ($c=5.206-0.20x$).¹³ The cathodoluminescence (CL) spectra were recorded at room temperature with an electron-beam energy of 15 keV. The RRS were measured in a backscattering configuration using the JYT64000 micro-Raman setup with a He–Cd laser (325 nm) as the excitation source, and the Raman shift was determined with good accuracy better than 0.6 cm^{-1} . The focused spot of laser on sample surface is about $10 \mu\text{m}$ with an incident power of 0.5 mW. The laser power was kept low to avoid laser heating of these alloyed nanostructures. According to studies by Alim *et al.*,^{11,12} this excitation intensity could only cause a LO phonon frequency redshift of about $< 1 \text{ cm}^{-1}$ due to local heating effect.

Figures 1(a) and 1(b) show the normalized RRS and CL spectra of the annealed samples (samples B–F), respectively. A consistent blueshift of the CL emission and “hot luminescence” emission¹⁴ in RRS were observed with increasing Mg composition. The inset of Fig. 1(b) shows the alloy band gap (E_g) as a function of Mg composition (x), obtained from RRS, photoluminescence (PL), and CL measurements. It is worth noting that the band gaps obtained by three different methods are consistent with each other. A good consistency between the experimental and theoretical results is shown in the inset of Fig. 1(b), in terms of the electronic structure

^{a)} Author to whom all correspondence should be addressed; electronic mail: yejd@ime.a-star.edu.sg

^{b)} Also at School of Electrical and Electronic Engineering, Nanyang Tech University, Singapore 639798, Singapore; electronic mail: exwsun@ntu.edu.sg

^{c)} Electronic mail: tripathy-sudhiranjan@imre.a-star.edu.sg

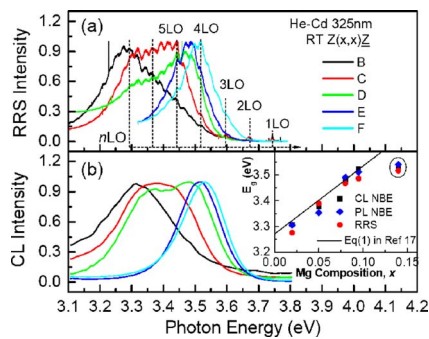


FIG. 1. (Color online) (a) Normalized resonant Raman scattering and (b) cathodoluminescence spectra of the annealed samples (samples B–F). The inset of (b) shows the dependence of band gap on the Mg composition, and the solid line represents the best fit to Eq. (1) in Ref. 15.

calculation¹⁵ and neglectable bowing effect for such small Mg fraction ($b=0$). For $x=0.14$, the shrinkage of band gap [Fig. 1(b)] compared to the simulation is possibly originated from band-tail states associated with the exciton localization and alloy potential fluctuations.¹⁶

Figure 2 shows the RRS of samples A–F. With increase in Mg composition, the dominated LO phonons exhibit three typical features: (i) the phonon peak shift toward higher energy side; (ii) the asymmetric broadening of the LO phonon line shapes; and (iii) the intensity enhancement of second- and higher-order LO phonons. These features are often observed in the case of polar alloy semiconductors and provide much physical information on the alloying effect and electronic state localization.³

The phonon spectra of alloy semiconductors generally exhibit frequency shift due to the reduced mass change of oscillating atomic pairs. In Fig. 2, the 1LO peaks show the segregation of ZnO LO mode and appearance of ZnO-like alloy LO mode with its frequency increasing from 578 to 607 cm^{-1} . The composition dependence of optical phonon frequency is shown as one-mode behavior, as predicted by the modified random-element-isodisplacement (MREI) model.^{9,17} The criterion for the existence of the one-mode pattern is that there must not be a substituting element whose mass (m) is smaller than the reduced mass (μ) of the compound formed by the other two elements.¹⁷ In $\text{Zn}_{1-x}\text{Mg}_x\text{O}$, since $m_{\text{Mg}}(24) > \mu_{\text{ZnO}}(12.8)$ and $m_{\text{Zn}}(65) > \mu_{\text{MgO}}(9.6)$, only one-mode behavior should be observed. Figure 3 shows the frequency of ZnMgO 1LO phonon as a function of Mg composition (x), together with the data from other literatures.^{7–9} Based on the MREI model, the composition dependence of LO phonon frequency can be expressed as the function of oscillator strength, force constants, and

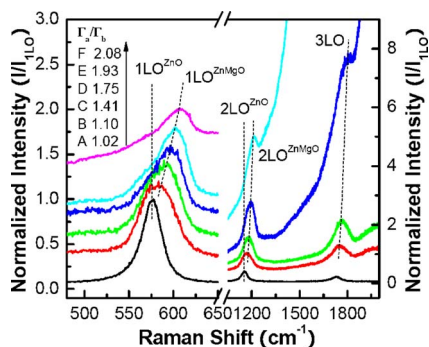


FIG. 2. (Color online) The RRS spectra of samples A–F. The asymmetry parameters of the 1LO phonon line shape are shown in the inset.

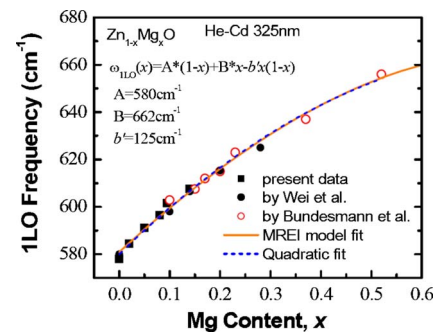


FIG. 3. (Color online) $\text{Zn}_{1-x}\text{Mg}_x\text{O}$ 1LO phonon line position as a function of alloy composition x ; the solid and dashed lines are the fits of MREI model and Eq. (1). The scattered data points are obtained from this study and Refs. 7–9.

dielectric response.¹⁷ The dielectric response function can be expressed as $\epsilon_{\infty}(x) = (1-x)\epsilon_{\infty}(\text{ZnO}) + x\epsilon_{\infty}(\text{MgO})$.¹⁷ Using $\epsilon_{\infty}(\text{ZnO})=3.7$ and $\epsilon_{\infty}(\text{MgO})=2.94$,⁹ our experimental data were fitted as shown in Fig. 3. The agreement between the theoretical model and our Raman data is excellent, and, moreover, the data derived from other literatures^{7–9} also match the model very well. To simplify the modeling process, we have derived a simple quadratic expression, similar to the band-gap determination with a bowinglike effect,

$$w_{1\text{LO}}(x) = w_{\text{ZnO}}(1-x) + w_{\text{MgO}}x - b'x(1-x). \quad (1)$$

Using Eq. (1), the present data can be well fitted (dashed line in Fig. 3) with w_{ZnO} and w_{MgO} of 580 and 662 cm^{-1} for the hexagonal ZnO and MgO, respectively. The bowing coefficient b' obtained as 125 cm^{-1} could be possibly due to the alloying disorder or strain effects. It is worth noting that the quadratic equation presents a perfect match to the experimental data of others^{7–9} and MREI model, even in the range of mixed phase of ZnMgO alloy ($0.33 < x < 0.5$). Thus, this nondestructive methodology provides a straightforward tool for determining the composition in wurtzite ZnMgO. Here we should emphasize that Raman shift of polar LO phonons owing to boundary confinement effect should be considered carefully if the surface-to-volume ratio is high or the size close to the exciton diameter of ZnO (~ 1.8 nm).^{18–20} As mentioned above in our case, the average sizes of ZnMgO nanocrystals are larger than 20 nm, and most of the collected light comes from the bulk volume and a small fraction from the boundary. Therefore, a small change in the shape of such ZnMgO nanocrystals may not lead to a detectable peak shift of the polar optical phonons.

Moreover, an anomalous enhancement in relative intensity for the second-order LO (2LO) phonon resonance is observed as the Mg composition increases (Fig. 2). In general, the strength of electron-phonon interaction would be weakened due to the very weak confinement effect in the grains larger than 20 nm. Also, the second-order structures are very sensitive to atomic scale disorder, and thus should be weakened by the increasing alloying compositional disorder. However, it is opposite in ZnMgO alloy nanostructures of our study. This effect can only be understood if the relevant resonance is the feature of extrinsic Fröhlich interaction mediated via a localized exciton. In fact, alloy-induced disorder is the main mechanism for exciton localization. The localized exciton would be excited with the absorption of the incident photon and relax into lower energy states with successive emission of LO phonons. The strong coupling of

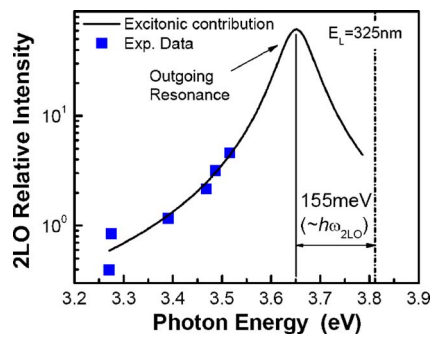


FIG. 4. (Color online) Relative intensity of 2LO as a function of the excitonic energy level. The square dots are experimental data and the curve represents a theoretical fit of Eq. (2).

exciton to the most energetic LO phonon results in the enhanced intraband Fröhlich contribution, and thus the second-order scattering would be enhanced greatly, as expected with the configuration model calculations.²¹ For such a cascade relaxation process, the Raman intensity of 2LO mode, based on exciton localization concept, can be described in a Lorentzian-like expression,³

$$I(2LO) = \frac{A}{2} \frac{z^4(1 - 2z^2 + z^4/4)}{[E_L - \hbar\omega(2LO) - \varepsilon] + \gamma^2}, \quad (2)$$

where A is the normalization constant, ε is the excitonic energy level, γ is the width of the localized exciton, z is proportional to the coupling constant of the localized exciton-phonon, and E_L is the incident photon energy ($\lambda=325$ nm). Since the room-temperature PL emission is mostly due to recombination of the donor-bound exciton in large size (>20 nm) ZnO and ZnMgO nanocrystals,²² the near-band-edge peak energy was used as the ε value, and the best fit between the experiment and the theory was obtained for $\varepsilon=3.659$ eV and $\gamma=52$ meV, as shown in Fig. 4. The estimated maximum intensity takes place for $\varepsilon=3.659$ eV, where 2LO phonon energy lies ~ 0.155 eV away from the incident photon energy of 3.814 eV (325 nm), indicative of an outgoing resonance. It is reasonable that the exciton binding energy in ZnMgO embedded nanocrystals is higher than the bulk ZnO because of the wider band gap and, therefore, the confinement effect may be significant due to potential fluctuation and localization. As the exciton binding energy is close to the LO phonon energy, a sharp resonance enhancement behavior will occur.²³ In fact, the density of these localized electronic states would also increase with the increasing alloy disorder and potential fluctuation in conduction band.³ This can be confirmed by the enhancement of fourth-order longitudinal optical (4LO) phonon resonance for sample F as shown in Fig. 1 where the energy difference between the incident and scattering phonon energies is ~ 0.298 eV [$\approx \hbar\omega(4LO)$]. Similar results can also be seen for the case of fifth-order longitudinal optical resonance. The weak outgoing feature for higher-order phonons may be due to the overlap of strong photoassisted hot luminescence and Raman broadening from alloy disorder effect.¹⁴

In Fig. 3, the LO phonon line shapes were broadened asymmetrically with a low-frequency tail developed at higher Mg composition as shown. The asymmetry parameter Γ_a/Γ_b defined as the ratio of half width at half maximum on the lower-frequency side (Γ_a) to that on the higher-frequency side (Γ_b) increases monotonically from 1.02 to 2.08, coupled with the increased broadening of line shapes (Fig. 3). This

phenomenon was generally attributed to the alloy potential fluctuation.^{4,6} The increasing potential fluctuation due to Mg composition will lead to the relaxation of the selection rule at $q=0$ and the activation of LO phonons with larger wave vector in the Brillouin zone. In addition, the localized excitons in real space would be delocalized in the Brillouin zone, resulting in a further strengthening of the exciton-mediated resonance process.²⁴

In summary, alloying effect and localized electronic states in $Zn_{1-x}Mg_xO$ nanocrystals (average size of 20–150 nm) have been studied using resonant Raman scattering spectroscopy. The anomalous enhancement of the 2LO phonon resonance is attributed to the extrinsic Fröhlich interaction via localized exciton as the intermediate electronic states. The dependence of the LO phonon peak energy on the Mg composition has been quantitatively studied, which provides a straightforward approach for determination of the alloy composition.

For supplemental materials, please see Ref. 25.

Financial support from the Agency for Science, Technology, and Research (A*STAR) Singapore, is gratefully acknowledged.

¹Y. R. Ryu, T. S. Lee, J. A. Lubguban, H. W. White, B. J. Kim, Y. S. Park, and C. J. Youn, *Appl. Phys. Lett.* **88**, 241108 (2006).

²A. Tsukazaki, A. Ohtomo, T. Kita, Y. Ohno, H. Ohno, and M. Kawasaki, *Science* **315**, 1388 (2007).

³C. Ramkumar, K. P. Jain, and S. C. Abbi, *Phys. Rev. B* **54**, 7921 (1996).

⁴F. Demangeot, J. Groenen, J. Frandon, M. A. Renucci, O. Briot, S. Clur, and R. L. Aulombard, *Appl. Phys. Lett.* **72**, 2674 (1998).

⁵P. Dua, S. L. Cooper, and K. Y. Cheng, *Appl. Phys. Lett.* **72**, 1072 (1998).

⁶H. Matsui, N. Hasuike, H. Harima, T. Tanaka, and H. Tabata, *Appl. Phys. Lett.* **89**, 091909 (2006).

⁷C. Bundsmann, A. Rahm, M. Lorenz, M. Grundmann, and M. Schubert, *J. Appl. Phys.* **99**, 113504 (2006).

⁸Z. P. Wei, Y. M. Lu, D. S. Shen, Z. Z. Zhang, C. X. Wu, J. Y. Zhang, B. Yao, and X. W. Fan, *Phys. Status Solidi C* **3**, 1168 (2006).

⁹J. Chen and W. Z. Shen, *Appl. Phys. Lett.* **83**, 2154 (2003).

¹⁰V. V. Zalamai, V. V. Ursaki, E. V. Rusu, P. Arabadji, I. M. Tiginyanu, and L. Sirbu, *Appl. Phys. Lett.* **84**, 5168 (2004).

¹¹K. A. Alim, V. A. Fonoberov, and A. A. Balandin, *Appl. Phys. Lett.* **86**, 053103 (2005).

¹²K. A. Alim, V. A. Fonoberov, M. Shamsa, and A. A. Balandin, *J. Appl. Phys.* **97**, 124313 (2005).

¹³S. Sadofev, S. Blumstengel, J. Cui, J. Puls, S. Rogaschewski, P. Schafer, Y. Dadpfev, and F. Henneberger, *Appl. Phys. Lett.* **87**, 091903 (2005).

¹⁴P. Y. Yu and M. Cardona, *Fundamentals of Semiconductors*, 3rd ed. (Springer, Berlin, 1999), Chap. 7, pp. 345–425.

¹⁵Y. S. Chang, C. T. Chien, C. W. Chen, T. Y. Chu, H. H. Chiang, C. H. Ku, J. J. Wu, C. S. Lin, L. C. Chen, and K. H. Chen, *J. Appl. Phys.* **101**, 033502 (2007).

¹⁶A. Ashrafi and Y. Segawa, *J. Vac. Sci. Technol. B* **23**, 2030 (2005).

¹⁷I. F. Chang and S. S. Mitra, *Phys. Rev.* **172**, 924 (1968).

¹⁸V. A. Fonoberov and A. A. Balandin, *Phys. Rev. B* **70**, 233205 (2004).

¹⁹V. A. Fonoberov and A. A. Balandin, *J. Phys.: Condens. Matter* **17**, 1085 (2005).

²⁰C. Nobile, V. A. Fonoberov, S. Kudera, A. D. Torre, A. Ruffino, G. Chilla, T. Kipp, D. Heitmann, L. Manna, R. Cingolani, A. A. Balandin, and R. Krahné, *Nano Lett.* **7**, 476 (2007).

²¹K. P. Jain, R. K. Soni, and S. C. Abbi, *Phys. Rev. B* **31**, 6820 (1985).

²²V. A. Fonoberov, K. A. Alim, A. A. Balandin, F. X. Xiu, and J. L. Liu, *Phys. Rev. B* **73**, 165317 (2006).

²³T. Makino, Y. Segawa, and M. Kawasaki, *J. Appl. Phys.* **97**, 106111 (2005).

²⁴A. Mascarenhas, M. J. Seong, S. Yoon, J. C. Verley, J. F. Geisz, and M. C. Hanna, *Phys. Rev. B* **68**, 233201 (2003).

²⁵EPAPS Document No. E-APPLAB-91-013735 for the supporting structural characterization data from these ZnMgO structures. This document can be reached via a direct link in the online article's HTML reference section or via the EPAPS homepage (<http://www.aip.org/pubservs/epaps.html>).